Climate Dynamics
https://doi.org/10.1007/s00382-020-05246-x

Influence of wintertime surface sensible heat flux variability over the central and eastern Tibetan Plateau on the East Asian winter monsoon

Lian Chen[1] · Renhe Zhang[1,2] · Sara C. Pryor[3] · Xiao Li[4] · Hui Wang[5]

Received: 2 December 2019 / Accepted: 13 April 2020

Abstract
Analyses of in situ and reanalysis output are performed to examine linkages between surface sensible heat fluxes over the central and eastern Tibetan Plateau (CETP) and indices of the East Asian winter monsoon (EAWM) and wintertime near-surface air temperatures over China. The results demonstrate that the sensible heat fluxes over CETP exhibit substantial decadal variability with positive, negative and positive phase during 1980–1987, 1988–2002 and 2003–2014, respectively. This decadal variability exhibits statistically significant associations with sub-components of EAWM and surface temperature anomalies over eastern China. The recovery of decadal change in wintertime sensible heat fluxes from negative to positive phase over CETP over the past decade (since 2003) has been associated with intensification and northward displacement of the East Asian subtropical jet (EASJ), enhanced and westward displacement of East Asian trough and strengthening of the Siberian High. Such processes are associated with the strengthening of EAWM, as well as cold air advection from high latitudes towards the south. Increased wintertime sensible heat fluxes over CETP is associated with markedly changes in the meridional temperature gradient that in term intensifies upper-level zone flow in the EASJ region, which provides a key physical factor linking the anomalies of sensible heat fluxes and EAWM.

1 Introduction

Heat and momentum exchanges between land and air over the Tibetan Plateau (TP) play an important role in dictating the atmospheric circulation, weather and climate over East Asia and globally (Duan et al. 2011; Fallah et al. 2016; Wu et al. 2007; Yanai et al. 1992; Ye and Wu 1998; Yeh 1950). Although some numerical simulations indicate that wintertime surface energy fluxes over TP are of secondary importance relative to the dynamic effect in terms of the impact on the regional climate (Wang and Wang 1985), the surface sensible heat flux (SH) is an important component of this forcing. For example, in winter, when SH is stronger in the areas of western TP, south TP valley and Hengduan mountainous, and weaker in the central-eastern TP (CETP), the Eurasian teleconnection pattern (EU) and Pacific/North American Pattern (PNA) are more prominent in 500 hPa geopotential height fields (Li et al. 2003). Intensification of SH over TP in winter is also associated with decreased winter temperatures in northwestern China and eastern coastal areas of mainland China (Yang and Li 2009). Accordingly, the magnitude of the SH over TP, its spatiotemporal variability and atmospheric response have been the subject of

Electronic supplementary material The online version of this article (https://doi.org/10.1007/s00382-020-05246-x) contains supplementary material, which is available to authorized users.

✉ Renhe Zhang
rhzhang@fudan.edu.cn

[1] Department of Atmospheric and Oceanic Sciences and Institute of Atmospheric Sciences, Fudan University, Shanghai 200433, China

[2] CAS Center for Excellence in Tibetan Plateau Earth Sciences, Chinese Academy of Sciences, Beijing 100101, China

[3] Department of Earth and Atmospheric Sciences, Cornell University, Ithaca, NY 14853, USA

[4] School of Atmospheric Sciences, Chengdu University of Information Technology, 610225 Chendu, China

[5] Key Laboratory of Meteorological Disaster, Ministry of Education (KLME)/Joint International Research Laboratory of Climate and Environment Change (ILCEC)/Collaborative Innovation Center on Forecast and Evaluation of Meteorological Disasters (CIC-FEMD), Nanjing University of Information Science and Technology, Nanjing 210044, China

Published online: 22 April 2020

extensive prior research (Chen et al. 2019; Duan et al. 2013; Huang et al. 2013; Shi and Liang 2014; Wang and Li 2019; Xu et al. 2009). Prior research has documented evidence that SH over TP declined from mid-1980s until the end of the century due largely to decreasing wind speeds, but that trend has subsequently reversed (Chen et al. 2019; Duan and Wu 2008; Yang et al. 2011; Zhu et al. 2017). These studies thus imply the possible presence of a decadal scale mode of variability, but to date there has been little research into the spatiotemporal characteristic of such a mode.

The East Asian winter monsoon (EAWM) is also an active component of the global circulation system (Chen et al. 2000; Ding 1994; Lau and Li 1984). Strong EAWM is associated with high-impact cold-air outbreaks over eastern China, Korea, Japan (Ding and Krishnamurti 1987; Huang et al. 2007; Jhun and Lee 2004; Wang et al. 2010; Wang and Chen 2009; Zhang et al. 1997). The EAWM as characterized by a range of indices applied to different reanalysis products also demonstrates variability on decadal and interdecadal timescales (Ding et al. 2014; Wang et al. 2009). It entered a weak phase starting in the late 1980s and strengthened since the mid-2000s (Wang and Chen 2014a). While potential drivers of this decadal variability have been previously investigated (Ha et al. 2012; Kim et al. 2017; Wang et al. 2009), the causes of EAWM decadal variations remain elusive. For example, Wang and Chen (2014a) suggested that enhanced wintertime blocking activity around the Ural mountain region and diminished Arctic sea ice concentration in the previous September are the responsible internal atmospheric process and external driver for the re-amplification of the EAWM in the mid-2000s, respectively. Wang et al. (2009) showed that the propagation and amplitude of quasi-stationary planetary waves also experience inter-decadal variations that are closely related to the weakening of EAWM in the late 1980s. While Ding et al. (2014) suggested inter-decadal variations in the ocean are an important influence on long-term variability of EAWM. The Northern Hemisphere Annular Mode/Arctic Oscillation (NAM/AO) is negatively correlated with EAWM (He et al. 2017), and the effect is modulated by the El Nino Southern Oscillation (ENSO) phase (Cheung et al. 2012). Gao et al. (2019) demonstrated that there are decadal changes in the impact of ENSO on the wintertime climate over East Asia. Other research has indicated the intensities of the East Asian trough and EAWM are linked to thermal forcing on TP (Wang and Wang 1985; Zhou et al. 2009).

Near-surface wintertime temperatures over eastern China exhibit decadal variations in time that are consistent with those present in SH over TP and EAWM (Ding et al. 2014; Huang et al. 2012; Kang et al. 2006; Lee et al. 2013; Wang et al. 2010; Wang and Lu 2017). For example, colder winters and significant negative surface temperature anomalies were observed during the recent strong EAWM epoch of 2004–2012. During this period, the wintertime temperature anomalies exceeded − 3 ℃ across a west-east swath of northern East Asia (Wang and Chen 2014a).

The objectives of the present work are to characterize decadal variability in SH over TP and to quantify the degree of the relationship between decadal variability in SH, intensity of EAWM and near-surface temperatures during the winter over China. This work is thus intended to advance our understanding of climate variability over TP and its links to the variability of winter climates over East Asia.

The rest of this manuscript is organized as follows. Section 2 describes the datasets and analysis methods. Spatiotemporal decadal variability of winter SH over CETP is analyzed in Sect. 3. Linkages between the decadal variability in winter SH over CETP and EAWM and temperature over China are examined in Sect. 4. In Sect. 5, we propose a possible mechanism that the SH over CETP affect EAWM and near-surface air temperatures. Finally, conclusions and discussions are presented in Sect. 6.

2 Datasets and analysis methods

The data used in the present study include the following:

(1) 6-hourly (0200, 0800, 1400 and 2000 LST at Beijing time, 8 h earlier than UTC) surface meteorological observations from 91 stations over the TP region (Fig. 1a). These data are used to derive a mean daily SH. They are collected, quality controlled and provided by the China Meteorological Administration (CMA) and comprise: air temperature at 1.5 m above ground level (a.g.l.) from a sheltered thermometer (Ta, in unit K), ground surface temperature at 0 cm (Tg, measured using a thermometer where one-half is horizontally exposed above ground, and the other half is horizontally interred, in unit K), wind speed at 10 m a.g.l. (V, in unit m s^{-1}) and station surface pressure (P, in unit Pa). As in our previous analyses (Chen et al. 2019), the bulk transfer method (Chen et al. 1985; Duan et al. 2011; Ye and Gao 1979) is used to derive estimates of SH:

$$SH = \rho C_p C_h |V|(T_g - T_a) \quad (1)$$

where C_p is the specific heat of dry air at a constant pressure (1004.07 J kg^{-1} k^{-1}); C_h is the bulk surface heat transfer coefficient. Although a wide range of values have been proposed for C_h over TP (Duan and Wu 2008; Li et al. 2002; Ye and Gao 1979; Zhang et al. 1988; Zhu et al. 2012), as in our previous research (Chen et al. 2019) a constant value of $C_h = 4 \times 10^{-3}$ is assumed; ρ, the air density (kg m^{-3}) can be calculated by:

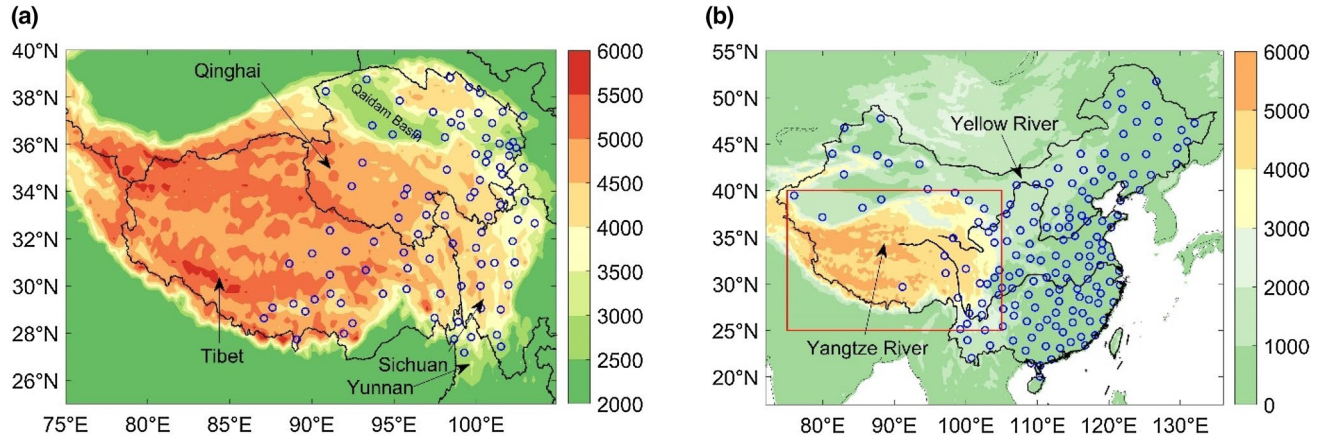

Fig. 1 Map of **a** the Tibetan Plateau (TP) region with terrain elevation (unit: m) and the locations of 91 stations (blue circles) used to characterize daily SH and **b** China with terrain elevation (unit: m) and 160 meteorological stations (blue circles) used to describe monthly surface air temperature. Frame of **a** shows a sub-set of the area (red rectangle) in (**b**)

$$\rho = P/R_d T_a \tag{2}$$

where R_d is the specific gas constant of dry air (287.05 J kg^{-1} k^{-1}). The four-times daily values are averaged to generate daily value at each station. Since only four stations are available over the western TP (west of 85°E), our study is focused on the central and eastern parts of TP (east of 85°E, hereafter called CETP).

(2) Monthly mean surface air temperature data from 160 meteorological stations in mainland China provided by CMA. This dataset, started in 1951, meets the World Meteorological Organization's standards and is updated every month to present. These stations are distributed across China but are concentrated in the eastern half of the country (Fig. 1b).

(3) Monthly mean sea level pressure (SLP), geopotential height, zonal and meridional wind components, and air temperature data at a horizontal resolution of 1.5° × 1.5° from European Center for Medium-Range Weather Forecasts (ECMWF) reanalysis (ERA-Interim) (Dee et al. 2011) started from 1979 are used to compute indices of EAWM. Chen et al. (2019) found that the ERA-Interim data is the best in accordance with the observed SH. The structure of the EAWM features distinct major components from lower troposphere to the tropopause. Thus, three indices are included in our analyses:

- "Upper tropospheric zonal wind shear over East Asia" index (Jhun and Lee 2004), defined as: Iu300 = U300 (27.5°–37.5°N, 110°–170°E) – U300 (50°–60°N, 80°–140°E), where U300 denotes the zonal wind speed at 300 hPa.
- "East Asian Trough" index (Cui and Sun 1999), defined as: Ig500 = mean (500 hPa geopotential heights over 35°–40°N, 110°–130°E). For ease of interpretation, Ig500 is multiplied by –1 with respect to its original definition so that a positive index corresponds to a strong EAWM winter.
- "pressure gradient" index (Wang and Chen 2014b): Islp = (2*SLP1-SLP2-SLP3)/2, where SLP1, SLP2 and SLP3 indicate the normalized area-averaged winter sea level pressure (SLP) over the Siberia (40°–60°N, 70°–120°E), North Pacific (30°–50°N, 140°E°–170°W) and Maritime Continent (20°S°–10°N, 110°–160°E).

Note that, all EAWM indices are normalized. Additional indices are also from ERA-Interim output; the meridional temperature gradient (MTG) derived using air temperatures on a range of geopotential surfaces, the 500−300 hPa thickness, and the 200 hPa zonal wind. These indices are also used to characterize dynamical linkages between the TP SH and large-scale circulations.

The observational period considered here spans 36 years from January 1980 to December 2015. The variable in each winter is calculated by averaging the monthly means in December, January and February (DJF) of a certain year, which result in 35 winters (1980–2014) where, for example, the winter of 2014 refers to December 2014−February 2015. Since the 91 stations used to computed daily SH are unequally spaced, we apply the method of Jones and Hulme (1996) using Thiessen techniques to develop regional area-weighted average records of monthly SH and those are averaged for winter in each year to generate a single value. Anomalies from the climatological mean are converted into Z scores by subtracting the mean and dividing by the standard deviation.

Rotated Empirical Orthogonal Function (EOF) analysis is applied to objectively extract spatial-temporal modes of variability in wintertime SH over CETP. Nine factors are retained for the rotation since the first nine modes explain over 69% of the total variance and the scree plot (not shown) becomes fairly flat after the tenth eigenvalue. The EOFs are rotated using the widely applied Varimax rotation algorithm (Kaiser 1958; Richman 1986). Ultimately, the first two modes of the rotated EOF (REOF) represent the most important variability of wintertime SH over CETP. Actually, the REOF results and the EOF results are very similar, indicating that the first two patterns are stable and physically meaningful. Herein, the spatial patterns are referred to as REOFs and the principal component scores (similarity indices to each REOF) (Richman 1986) are referred as RPCs.

Relationships between winter patterns of SH over CETP and temperature patterns in China are analyzed using Singular Value Decomposition (SVD) (Naoto and Wallace 1995). This technique seeks to objectively identify and compare coupled modes based on maximizing covariance between the expansion coefficients of the leading pattern in each field (Bretherton et al. 1992; Wallace et al. 1992). To highlight the decadal variability, we use a low-pass recursive Butterworth filter (cut off period of 9-years) to obtain the low frequency of a time series. Regression and Pearson correlation analyses are conducted to characterize linear relationships between climate indices and measures of SH over CETP, and a two-tailed Student's t-test is used to assess statistical significance (Wilks 2011).

3 Spatiotemporal variability of winter SH over CETP

The REOF analysis is applied to the SH anomalies over CETP, and the spatial distributions of the first and second REOF modes as well as their principal components (PCs) are shown in Fig. 2. Based on the method of North et al. (1982), the two modes are significantly separable. The leading mode in wintertime SH anomalies (REOF1, Fig. 2a) is characterized by positive SH anomalies over most parts of CETP. There is a small region of weak negative anomalies to the south of 30°N in the western portion of the region and in the north of Yunnan province. Time series of the principal

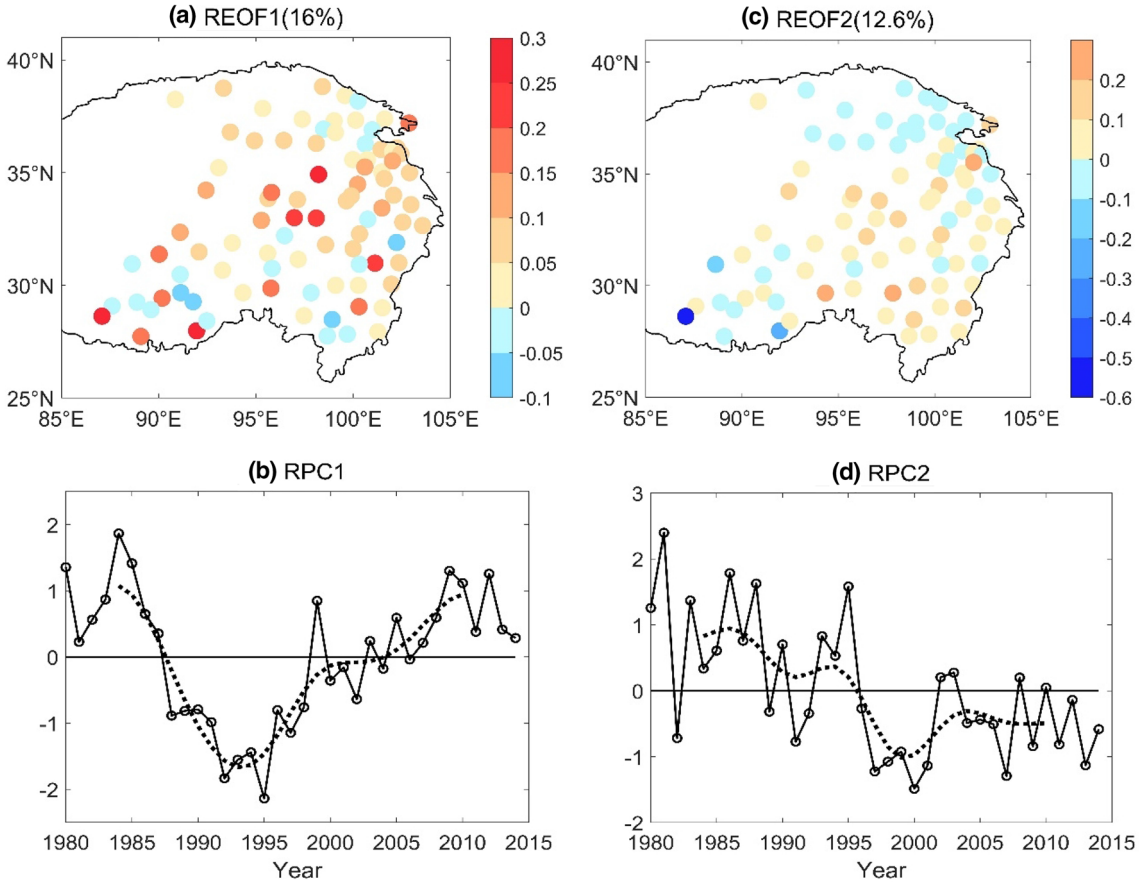

Fig. 2 Spatial patterns (**a**, **c**) and corresponding time series (**b**, **d**) of the first two leading REOFs of wintertime SH anomalies over CETP during 1980–2014. The dot-dashed lines in (**c**, **d**) indicate thedecadal curves obtained by Butterworth filter with a period of 9-years

component for this mode (RPC1, Fig. 2b) indicates the evidence of decadal variability with positive phase from the early 1980s to mid-1980s, following by negative phase from 1988 to the beginning of 2000s (1988–2002). After 2003, RPC1 was consistently positive. This decadal oscillation feature is particularly obvious when a decadal Butterworth filter is applied (Fig. 2b). The resulting time variation implies the declines until the mid-1990s followed by a consistent tendency towards increasingly positive values.

To further prove the decadal variability of SH over CETP as demonstrated by RCP1 (Fig. 2b), we show in Fig. 3a the time evolution of the area-weighted average of SH over CETP. It can be seen that the positive decadal phases appeared before 1987 and after 2003, and negative phase in 1988–2002, which are well in consistency with those reflected by RCP1. Based on the sign of RPC1 from the leading REOF as well as the decadal variation of the area-weighted average of SH over CETP, the time series of wintertime SH from each of the 91 stations is divided into three segments, i.e., 1980–1987, 1988–2002 and 2003–2014. Considering the decadal component of SH exhibited almost an entire cycle during 1988–2014 (Figs. 2b and 3a), a difference is computed between the period of 2003–2014 in the positive phase of the SH decadal variability and that of 1988–2002 in the negative phase. The resulting difference field shows positive anomalies in wintertime SH of up to 27 W/m^2, relative to a long-term mean wintertime value of approximately 30 W/m^2 (Chen et al. 2019) over much of CETP in the latter period, with a smaller area of negative anomalies in the west of Sichuan province (Fig. 3b). The spatial pattern of the difference in SH between the latter and earlier periods is similar to REOF1 (Fig. 2a). Spatial correlation coefficient between these two fields is 0.74, which exceeds the 0.001significant level.

The second leading mode (REOF2, Fig. 2c) of winter SH over CETP is characterized by positive loadings over the central and southeastern TP, and negative loadings to the northeastern and southwestern TP. The PC scores from the second component (RPC2, Fig. 2d) are positive during 1980–1995, and then become predominantly negative (Fig. 2d), leading to a negative linear trend of 0.06 per year, which is statistically significant exceeding the 0.01 significant level.

This analysis thus further indicates the presence of significant decadal modes of variability in winter SH over CETP, consistent with the results of Xie et al. (2018) and Chen et al. 2019)

4 Linkages between decadal variability in winter SH over CETP, EAWM and near-surface temperatures over China

4.1 Wintertime SH over CETP and near-surface air temperatures over China

A first order assessment of the degree of association between decadal variation of wintertime SH and near-surface temperature over China is derived by regressing the winter air temperature at the 160 stations in China against RPC1 of wintertime SH. The regression slopes are negative and exceed the 0.05 significant level over most of China, indicating that years with positive SH anomalies are associated with statistically significant negative temperature anomalies except over TP (Fig. 4a). The regression coefficients are particularly large over northeastern, north China and Yangtze-Huai river basin, and are small (and positive) over TP. The composite difference in wintertime temperatures (2003–2014 minus

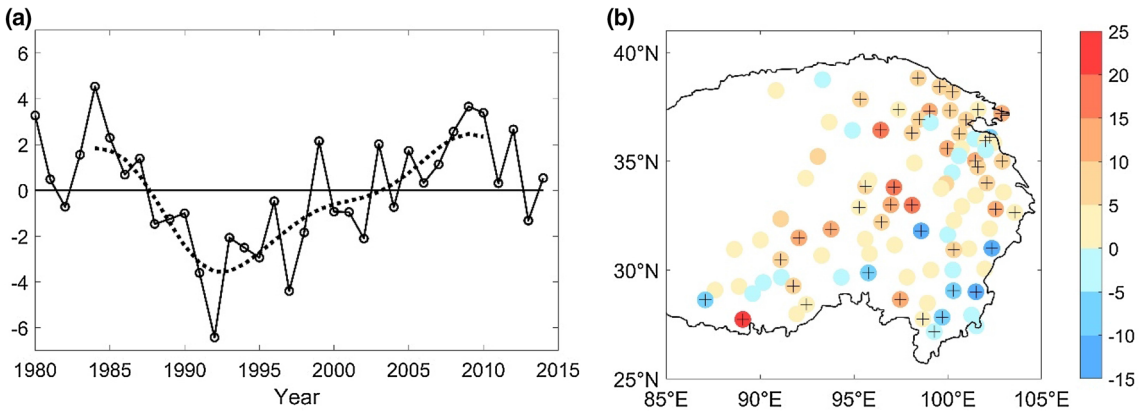

Fig. 3 **a** Time evolution of the area-weighted average of wintertime SH over CETP from 1980 to 2014 and **b** composite difference in mean wintertime SH over CETP (2003–2014 minus 1988–2002) (unit: W/m^2). The dot-dashed line in (**a**) indicates the low frequency curve by Butterworth filter with a period of 9-years. The circles with black cross in (**b**) indicate the difference exceeding the 0.1 significant level determined by a two-tailed Student's t-test

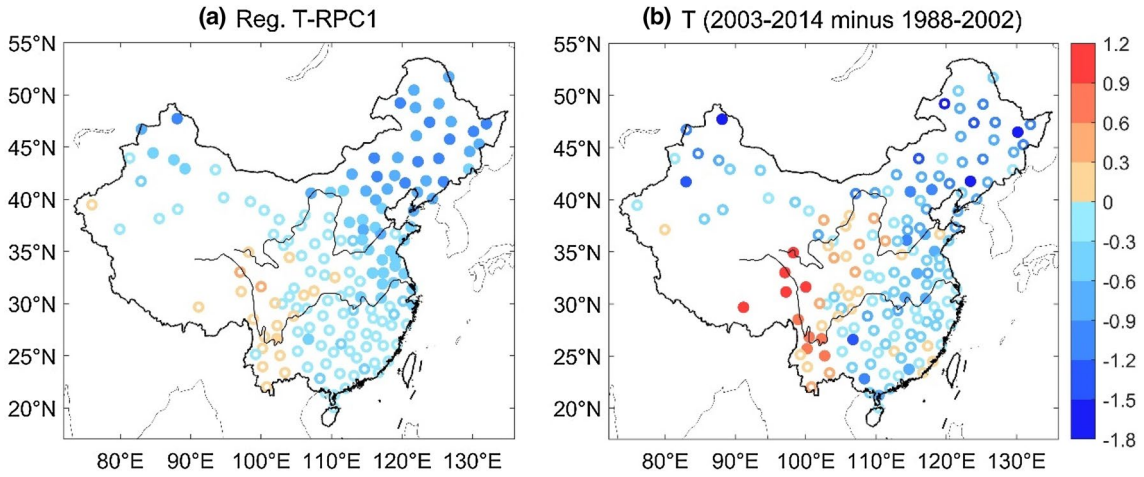

Fig. 4 **a** Slope of regression fits of wintertime near-surface temperature to RPC1 of SH over CETP. **b** Composite difference of winter surface air temperature (2003–2014 minus 1988–2002) (unit: K). The filled circles indicate the values exceeding the 0.05 significant level determined by a two-tailed Student's t-test

1988–2002) exhibits a similar spatial pattern (Fig. 4b). Thus, lower SH over CETP during 1988–2002 were associated with above average wintertime temperatures over most of China. In contrast, the transition to higher SH after the early 2000s was associated with lower wintertime temperatures particularly over the eastern part of China. The sensible heat flux over the eastern Tibetan Plateau is weakly related to the in situ surface air temperature. This may be because the surface temperature is determined not only by SH, but also by many other elements, such as temperature advection, solar shortwave radiation, surface longwave radiation, etc.

To further substantiate the link between wintertime SH over CETP and temperature over China, a SVD analysis is performed based on the covariance matrices of decadal variation of the two fields. The results are displayed as homogeneous correlation patterns (Fig. 5), because these patterns show the degree to which the fields are related and how much of the variation amplitude can be explained by the SVD modes (Wallace et al. 1992). The first SVD mode accounts for 69% of the total covariance between the two fields and the temporal coefficient between the two field expansion coefficients in the first mode is 0.9, indicating the two fields are significantly positively correlated. The homogeneous correlation maps of the first SVD mode are shown in Fig. 5 for wintertime SH and temperature, respectively. This mode represents 26% of the total SH variance, and is characterized by a uniform pattern with significant positive correlations over most of CETP (Fig. 5a). The first SVD mode of temperature, which accounts for 58% of the temperature variance, shows large uniformly negative

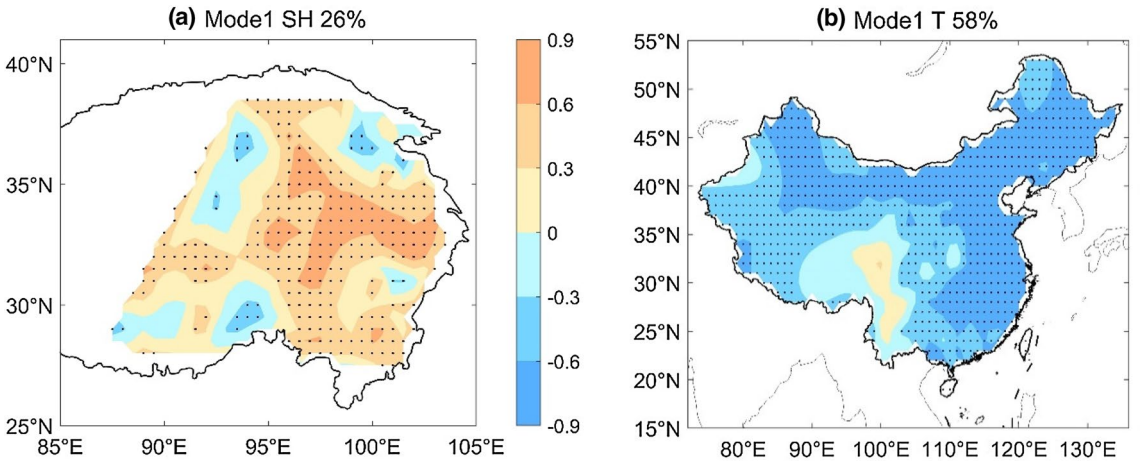

Fig. 5 Heterogeneous correlations of the first SVD mode of decadal components of wintertime **a** SH and **b** temperature anomalies. Black dots denote areas with statistical significance exceeding the 0.05 significant level determined by a two-tailed Student's t-test

correlations except over the Tibetan Plateau (Fig. 5b). This mode is exhibits spatial similarity with the first EOF mode of winter temperatures over China (Hu et al. 2015), further emphasizing the connections between decadal variations in wintertime SH over CETP and near-surface temperatures over most of China.

SVD is also performed to examine the linkage between the inter-annual variability of wintertime SH and temperature anomalies using the unfiltered time series. The heterogeneous correlation patterns of the first SVD mode (figures are not shown) are similar to those in Fig. 5, indicating that the negative correlation between SH over CETP and temperature over east parts of China exist at both the inter-annual and decadal timescales. Using low and high frequency variability of SH and temperature anomalies, we compare the statistics of the first SVD mode, including the explained percentage of total covariation, explained variation in individual field, and temporal correlation between pairs of expansion coefficients respectively (Table 1). All statistical metrics are larger for decadal (filtered) time series, indicating that the relationship between SH over CETP and temperature over China is closer on thedecadal timescale than inter-annual timescale.

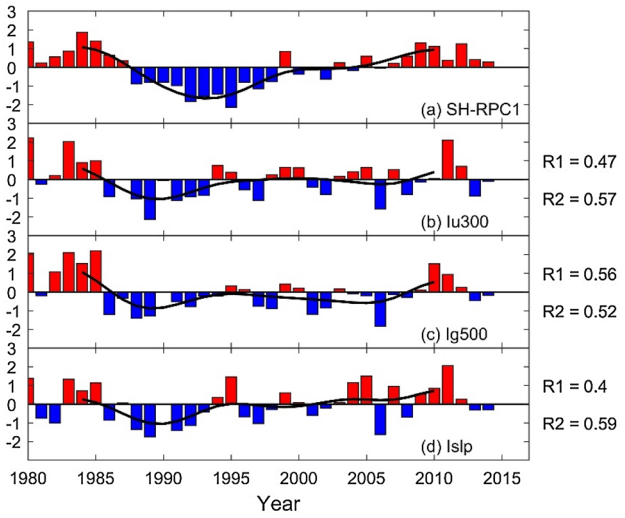

Fig. 6 **a** RPC1 of winter SH over CETP and **b–d** normalized anomalies of EAWM index (bar) based on different definitions for the period 1981–2014. The lines indicate 9-year low-pass components using Butterworth filter. R1 and R2 are correlation coefficients of the corresponding EAWM index with RPC1 of wintertime SH before and after extracting decadal variability, respectively

4.2 Wintertime SH over CETP and the EAWM

Time series of the three EAWM indices and RPC1 of the wintertime SH are given in Fig. 6. All three EAWM indices (Iu300, Ig500 and Islp) exhibit decadal variability. Consistent with the previous study of Ding et al. (2014) these indices indicate EAWM weakened during 1986/87–2004/05 and subsequently strengthen after 2005. The correlation coefficients of RPC1 with Iu300, Ig500 and Islp are 0.47, 0.56 and 0.4, respectively, exceeding the 0.05 significant level. It is indicated that all EAWM indices and RPC1 exhibited similar long-term variability with a dominance of negative values during 1988–2002 and positive values in the period before 1987 and after 2003. When a Butterworth filter with a period of 9-years is applied to the time series, the correlations of Iu300 and Islp with RPC1 are even higher, indicating that the decadal variability in SH over CETP is closely linked to recent re-amplification in EAWM. We further calculate the decadal variances of Iu300, Ig500 and Islp explained by RPC1, which are 28.09%, 37.21%, and 31.36%, respectively. Therefore, nearly 1/3 variance of the decadal EAWM variation can be explained by SH over CETP, indicating the important role played by SH over CETP in the decadal variability of EAWM.

The composite difference fields (2003–2014 minus 1988–2002) in the variables for the EAWM indices illustrate the spatial manifestations of the changes in EAWM (Fig. 7). Climatological zonal wind field over East Asian region indicates that during winter, there is a zonally extended westerly East Asian subtropical jet (EASJ) south of 40°N and a weaker East Asian polar front jet (EAPJ) to the north of TP associated with westerly and northwesterly winds (Ren et al. 2010). Generally, a strong EASJ is associated with intensification of large-scale circulations, such as the Siberian High and East Asian trough and an intensified EAWM (Ha et al. 2012; Jhun and Lee 2004; Zhang and Xiao 2013). The difference in zonal winds at 200 hPa (2003–2014 minus 1988–2002) indicates a tri-pole alternating pattern meridionally and that during the later period (with higher SH over CETP) there were strengthened zonal winds around 25°–40°N and weakened winds to the north and south of TP, especially in the 50°–70°N latitude band (Fig. 7a). This

Table 1 The total variation contribution, variation contribution for decadal (inter-anual) variability of SH over CETP and temperature, and correlation coefficient between the two field expansion coefficients resulting from the first SVD mode

	Total variation contribution	SH variation contribution	Temperature variation contribution	Correlation coefficient
Decadal	69%	26%	58%	0.9
Inter-annual	64%	15%	47%	0.72

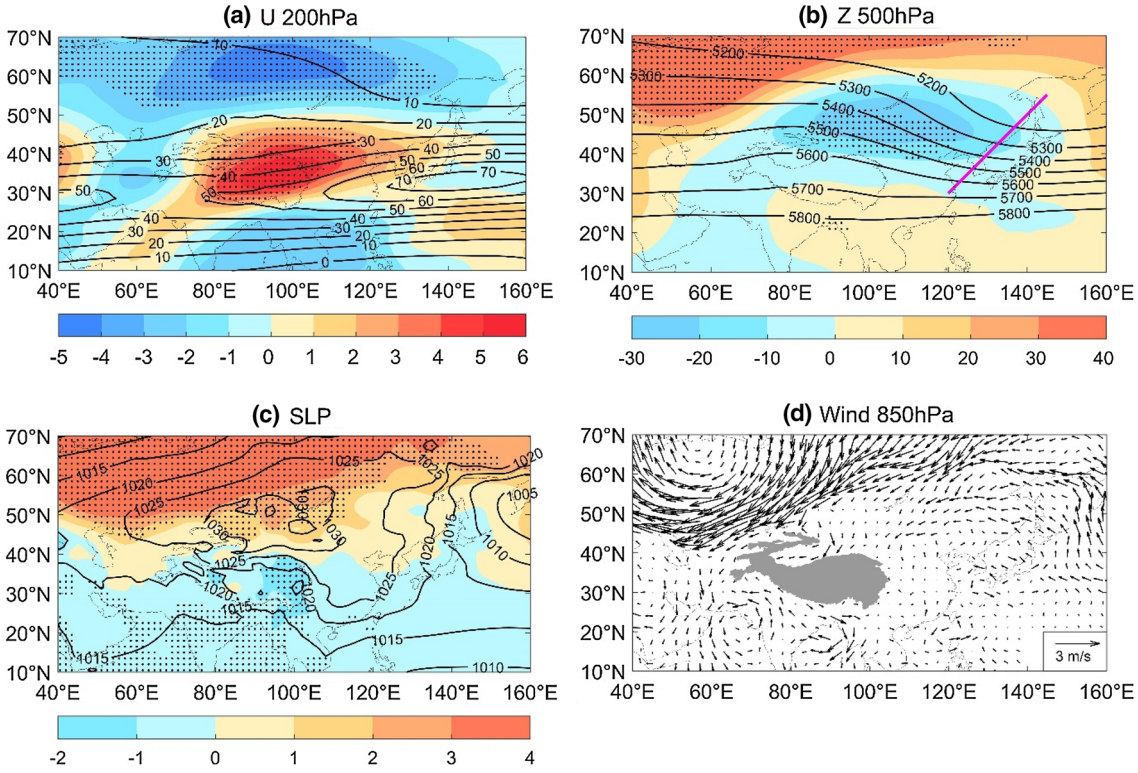

Fig. 7 Composite differences between periods of 2003–2014 and 1988–2002 for **a** zonal winds at 200 hPa (unit: m/s), **b** geopotential heights at 500 hPa (unit: gpm), **c** sea level pressure (unit: hPa) (shadings), and for **d** winds at 850 hPa (unit: m/s) (vectors). Contours in (**a**–**c**) represent climatological DJF means of corresponding variables. Black dots indicate areas in which the composite differences exceed the 0.05 significant level determined by a two tailed Student's t-test. The magenta line in figure **b** indicates the approximate mean orientation of the East Asian trough in 500 hPa geopotential heights during winter

negative-positive-negative pattern of zonal wind anomalies from 10°N to 70°N leads to a weaker East Asian polar front jet (EAPJ) and a stronger and pole-ward East Asian subtropical jet (EASJ) during stronger SH period.

The change in the large-scale circulation (2003–2014 minus 1988–2002) is also evident in the 500 hPa geopotential heights (Fig. 7b). The latter period is characterized by lower geopotential heights (~ 25 gpm) over 40°–60°N and 90°–130°E (i.e. the Baikal region and northeast Asia) (Fig. 7b). These height anomalies deepen the East Asian trough and move it westward. The corresponding anomalous cyclonic circulation helps to strengthen the northerly wind flow from the high latitudes into eastern China, leading to stronger EAWM and colder winter.

The corresponding difference in sea-level pressure (SLP) (2003–2014 minus 1988–2002) indicates large positive SLP anomalies dominate northern Eurasia (Fig. 7c), associated with strengthening of the Siberian High and expansion poleward. In the composite difference of 850 hPa wind field between the two periods (Fig. 7d), a striking feature is that an anomalous anticyclone appears over northern Eurasia, in consistency with the increased geopotential heights (Fig. 7b) and positive pressure anomalies in SLP (Fig. 7c). The anomalous anticyclone is an evidence of the strengthened Siberian High, which has major impact on EAWM.

The slope of regression fits of the EAWM indices and the RPC1 from the wintertime SH fof CETP (Fig. 8) exhibits similar spatial patterns to the composite difference fields between the stronger and weaker SH periods (Fig. 7), suggesting that the circulation changes between the two periods are closely linked to wintertime SH over CETP. Positive SH anomalies over CETP are associated with changes in the atmospheric circulation that characterizes the three-dimensional structure of EAWM: strengthening of the upper-level jet stream, deepening and displacement of the 500 hPa East Asian trough, and intensification and shifting the Siberian High (as manifested in the SLP field). Positive SH anomalies over CETP are thus manifested as strengthening the EAWM and cold conditions over central and eastern China.

It should be noted that there are some differences between the composite difference fields and regression patterns (Fig. 7 vs. Fig. 8). For example, in the mid-troposphere, difference field of geopotential heights at 500 hPa (Fig. 8b) represent the westward displacement of East Asian trough with anomalous low over Lake Baikal, while the regression pattern is characterized not only by westward shift but also

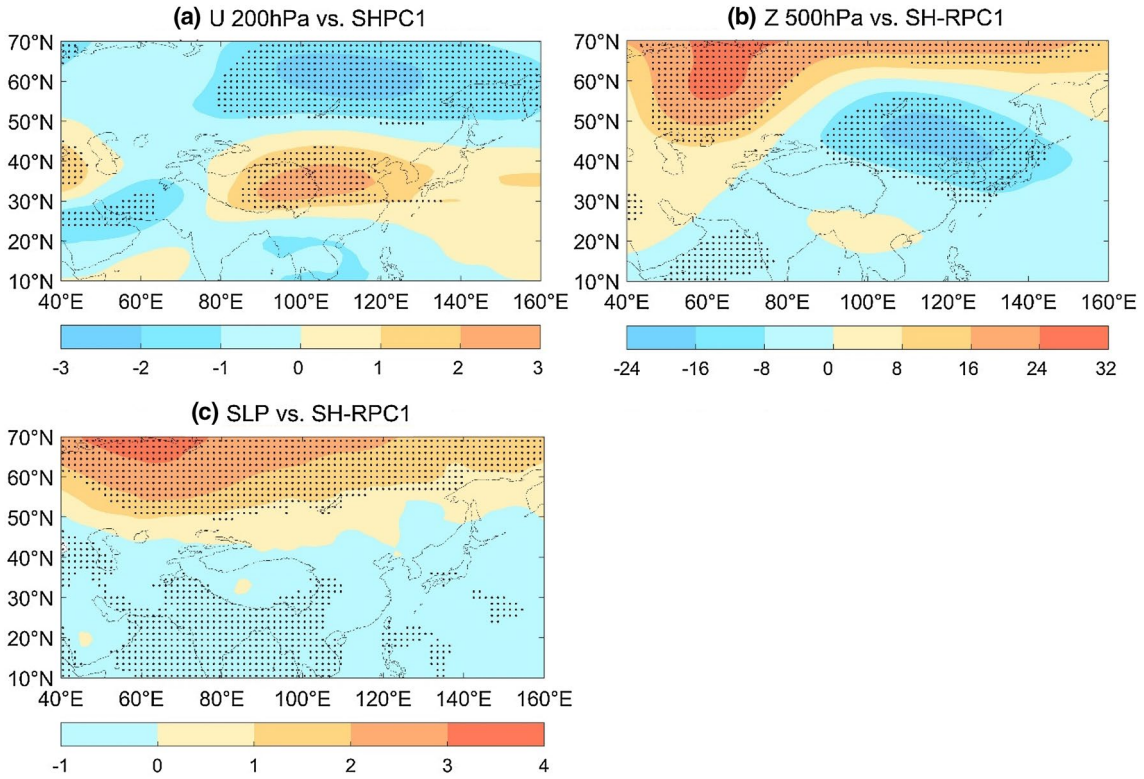

Fig. 8 Regression slopes of **a** zonal winds at 200 hPa (unit: m/s), **b** geopotential heights at 500 hPa (unit: gpm) and **c** sea level pressure (unit: hPa) with respect to the RPC1 of wintertime SH. The dotted areas indicate the regression slopes exceeding the 0.05 significant level

deepening of East Asian trough with negative anomalies along the East Asian trough axis. This difference probably implies the signal in 1980–1987. The composite difference field is focus on the circulation change between period of 2003–2014 and 1988–2002, which mainly reflects the northern mode of EAWM (Leung and Zhou 2015; Wang et al. 2010). Meanwhile, the regression pattern implies the circulation changes linked to wintertime SH over CETP during the whole study period, including the feature in 1980–1987, which is consistent with the results of Wang and Chen (2014a). The 500 hPa geopotential heights averaged over 30°–50°N, 110°–130°E (green box in Fig. 9b) is a reasonable index for well measuring both the northern and southern modes (Wang et al. 2010). The pronounced

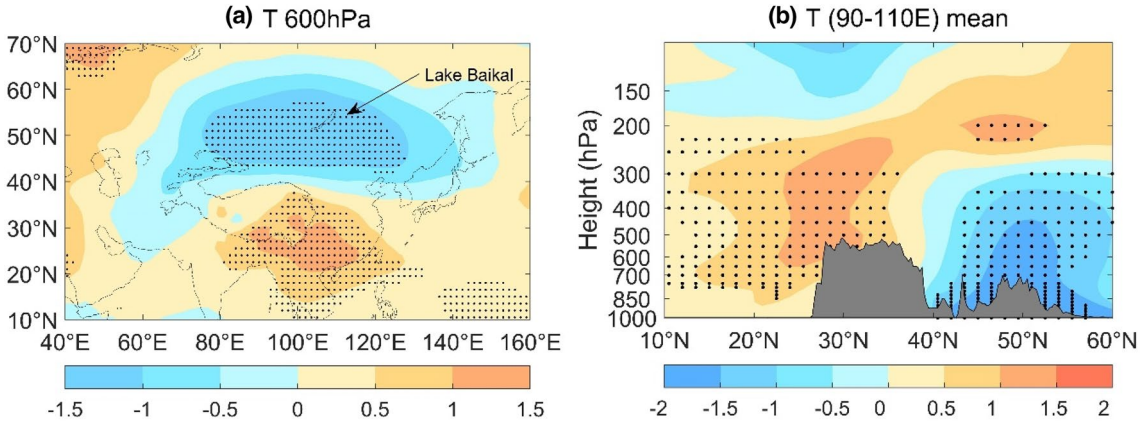

Fig. 9 The composite difference of winter air temperature between 2003–2014 and 1988–2002 **a** at 600 hPa and **b** in vertical-latitude cross-section along 90°–110°E (unit: K). The dotted areas indicate the difference is significant exceeding the 0.05 significant level according to a two tailed Student's t-test. The gray shaded areas in (**b**) indicate the topography

relationship, with the correlation coefficient 0.7, between SH anomalies over CETP and this index suggests that SH anomalies over CETP are associated with changes in the atmospheric circulation that characterizes the spatiotemporal structure of EAWM.

5 Possible mechanisms for the SH over CETP affecting the EAWM

The above analyses suggest that the variations of decadal variability in wintertime SH over CETP in recent decades are significantly linked to the decadal variability in both the EAWM circulation and near-surface temperatures over eastern China. In this section, we seek to explore and describe the primary physical mechanisms responsible for this linkage.

Consistent with *a priori* expectations, the thermal structure of the atmosphere in the vicinity of TP is strongly influenced by SH over the plateau. For example, the composite difference in wintertime temperature at 600 hPa (the average pressure on the TP) between 2003–2014 and 1988–2002 indicates considerably higher temperatures (by up to 1.5 K) in the later period over CETP, and cooler conditions over the north Asia region, centered on Mongolia and the region near Lake Baikal (Fig. 9a). The latitude-vertical cross-section (Fig. 9b) indicates the higher temperatures over TP during 2003–2014 (when the SH was higher) extended from the TP surface (600 hPa) to 200 hPa and the sign reverses in stratosphere. Meanwhile, the center of lower temperatures over the area north of Plateau extends into the mid to high troposphere (up to 300 hPa).

The change in SH is associated with a change in the meridional temperature gradient (MTG) which can affect the large scale circulation. Defining the meridional temperature gradient (MTG) using thickness of the 500–300 hPa layer as a proxy for the mean temperature, the MTG is estimated as $\frac{\Delta T}{R\Delta\varphi}$, where ΔT is the difference of the 500–300 hPa thickness over a latitude band $\Delta\varphi$, and R = 6371 km is the earth's radius. A positive MTG thus corresponds to temperature decrease with latitude. Consistent with the discussion above, the difference in MTG (2003–2014 minus 1988–2002) shows higher values north of CETP (centered around 30°–45°N, extending from TP to the south of Lake Baikal) in 2003–2014 (Fig. 10a). Conversely, the difference in MTG (2003–2014 minus 1988–2002) is negative over mid-high latitude parts of Asia (around 55°–70°N) and the region to the south of eastern TP. Consistent with decadal difference of MTG between 2003–2014 and 1988–2002 (Fig. 10a), the regression slope of MTG on RPC1 of the CETP SH shows a tri-pole zonal pattern of meridional 500–300 hPa thickness gradient with negative-positive-negative anomaly from low latitude to high latitude (Fig. 10b). This suggests that the decadal change of MTG between the two periods is closely linked to the recent recovery of decadal change in wintertime SH from negative to positive phase over CETP.

The change in SH and associated change in the MTG affect the large scale circulation and specifically the zonal winds through the thermal-wind relationship (Wallace and Hobbs 2006). Figure 11 shows the standardized anomalies of MTG and zonal wind speed at 200 hPa averaged over the latitude band within a rectangle 90°–105°E and 10°–70°N (shown in Fig. 10b) during the two time periods 1988–2002 (P1) and 2003–2014 (P2). It is clear that differences in the meridional displacement, intensity and phase of the MTG between 2003 and 2014 and 1988–2002 are closely associated with changes in the zonal winds at 200 hPa. This implies that variations in the SH over CETP and the resulting changes in the MTG are dynamically linked to variations in the 200 hPa zonal winds and thus the westerly jet.

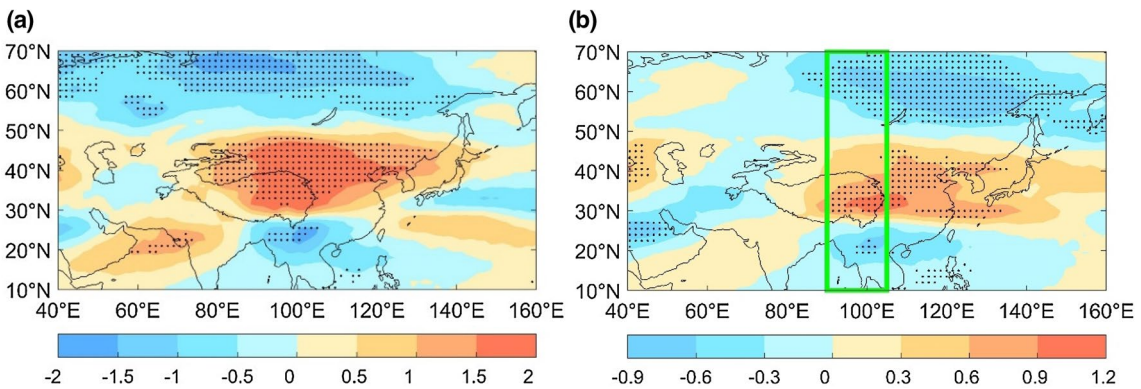

Fig. 10 **a** The decadal change in meridional 500–300 hPa thickness gradient (unit: 10^{-5} gpm/m) between 2003 and 2014 and 1988–2002. **b** Regression slopes of meridional 500–300 hPa thickness gradient against RPC1 of wintertime SH over CETP (unit: 10^{-5} gpm/m). The dotted areas indicate the values exceeding 0.05 significant level according to a two-tailed Student's t-test

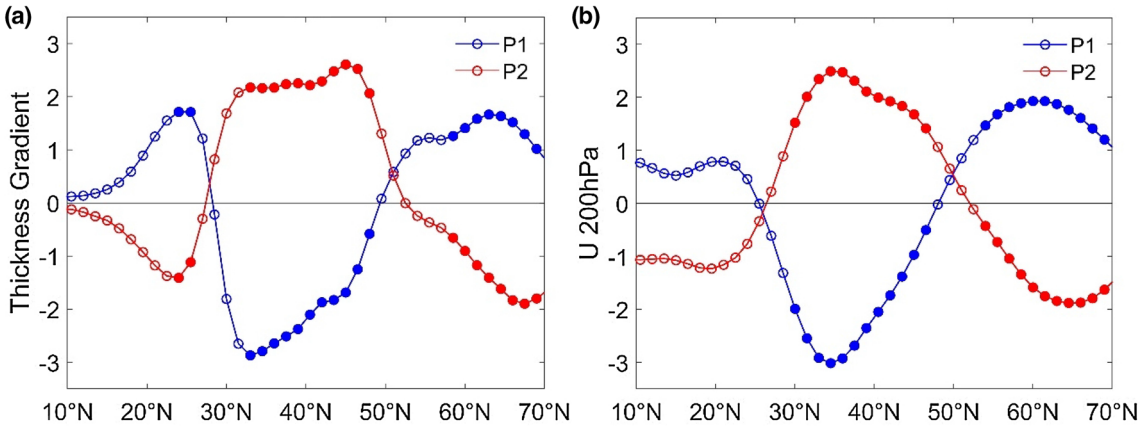

Fig. 11 The variations of **a** the standardized MTG (expressed as a thickness gradient) and **b** zonal winds at 200 hPa in different latitude bands averaged over 90°–105°E in 1988–2002 (P1) and 2003–2014 (P2). The filled circles indicate the difference between P1 and P2 exceeding the 0.05 significant level according to a two-tailed Student's t-test

Generally, a strong EASJ is associated with intense large-scale circulations, and is a key physical factor linking SH over CETP and the EAWM. In the region (90°–105°E, 30°–40°N) of significant difference in MTG between the high and low SH periods, we define a intensity index of EASJ (Ieasj) as the regional mean westerly winds at 200 hPa where |U| >=30 m/s in each winter. This index (Ieasj) exhibits a Pearson correlation coefficient of 0.47 with wintertime SH over CETP, which is statistically significant exceeding the 0.05 significant level. It is indicated that the intensity of EASJ is significantly linked to wintertime SH over CETP. Slope coefficients from regression fits between Ieasj and EAWM components (geopotential heights at 500 hPa, SLP and meridional winds at 850 hPa) (Fig. 12) and

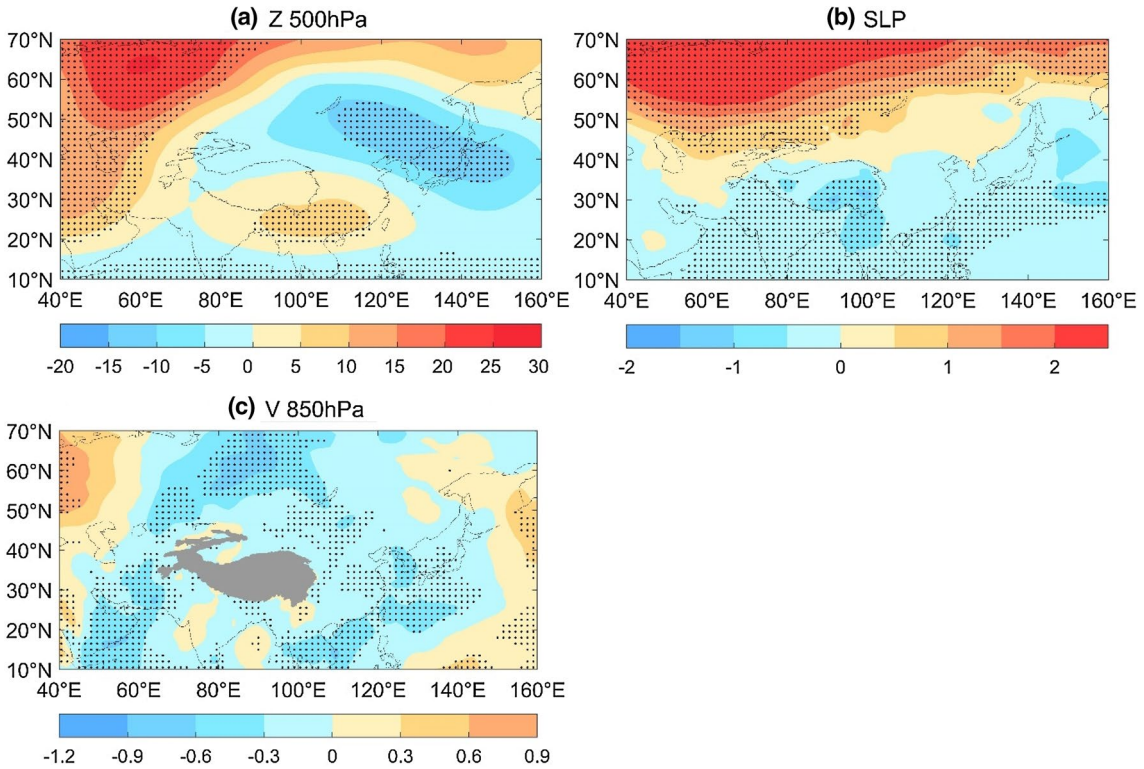

Fig. 12 Regression coefficients of **a** geopotential heights at 500 hPa (unit: gpm), **b** sea level pressure (unit: hPa) and **c** meridional winds at 850 hPa (unit: m/s) with respect to the intensity index of EASJ. The dotted areas indicate regression slopes exceed the 0.05 significant level according to a two-tailed Student's t-test. The grey region in (**c**) is the TP

Pearson correlation coefficients between Ieasj and EAWM indices (Table 2) indicate that strengthening of the EASJ is associated with decreased 500 hPa geopotential heights from Lake Baikal to Japan (with correlation coefficient 0.6 between Ieasj and Ig500), leading to westward displacement and intensification of the East Asian trough. The positive SLP anomalies over high-latitude Eurasia suggest that the strengthening of Siberia High is closely linked to strengthening of the EASJ and northerly winds at 850 hPa. As shown in Table 2, the strength of EASJ has statistically significant linkages to all EAMW indices, and all descriptors of EAWM are also significantly correlated to each other with correlation coefficients larger than 0.45. These results are consistent with previous research that has linked EAWM variability to the upper-level westerly jets (Luo and Zhang 2015).

6 Conclusions and discussions

This study analyzed the decadal variability in sensible heat flux (SH) over the central-eastern Tibetan Plateau (CETP) (computed using in situ data) and assessed its connection to the observed near-surface temperatures over China, and upper-air variables and indices of East Asian winter monsoon (EAWM) computed from the ERA-Interim reanalysis. The main conclusions are summarized as follows.

(1) From 1980 to 2014, winter SH over CETP exhibited substantial decadal variability. Rotated Empirical Orthogonal Function (REOF) analysis applied to the spatial fields of wintertime SH resolves a first mode that is characterized by positive SH anomalies over most parts of CETP and exhibits a decadal variation with negative, positive and negative phases during 1980–1987, 1988–2002 and 2003–2014, respectively. Such decadal variability is also proved by using the time evolution of the area-weighted average of wintertime SH over CETP from 1980 to 2014.

(2) The spatial pattern of the first REOF mode for wintertime SH anomalies exhibits high similarity with that of the composite difference of wintertime SH between 2003 and 2014 and 1988–2002, and is negatively correlated with near-surface air temperatures over central and eastern China. Thus, the recent transition to higher positive principal component scores of the first REOF mode (RPC1) (and increased SH) is associated with an increased likelihood of cooler wintertime temperatures over much of China. The time series of RCP1 (from the wintertime SH anomalies) is correlated with indices of the EAWM. The evidence is presented that positive wintertime SH anomalies over CETP are associated with intensification and northerly shift of the subtropical westerly jet. Further, the East Asian trough (characterized using 500 hPa geopotential heights in the trough region) is enhanced and exhibits westward shift. The Siberian High (as manifest in the SLP field and anomalous anty-cyclone at 850 hPa) is also stronger during the period of higher SH, demonstrating a typical intensified EAWM. The strengthening of northern wind anomalies further triggers the cold air southward, resulting in cold winters over eastern China.

(3) A possible mechanism by which SH over CETP physically links to the variables (near-surface temperatures and the components of EAWM) is elaborated. The adiabatic heating anomaly associated with the decadal change in SH over CETP alters the atmospheric circulation by altering the meridional temperature gradient and hence the atmospheric baroclinicity. Air temperatures at 600 hPa over the main and southern region of TP were higher while those over North Asia-north of TP were significantly lower during 2003–2014 than during 1988–2002. Such meridional anomalous feature of temperatures extended from the surface of TP to the upper troposphere, leading to enhancement of the SH-induced meridional 500–300 hPa thickness (temperature) gradient especially in the region (90°–105°E, 30°–40°N). Accordingly, the zonal winds at 200 hPa in this region were accelerated, resulting in the enhanced intensity of EASJ, and a strengthened EAWM.

Table 2 Pearson correlation coefficients of the intensity index of EASJ (Ieasj) with the EAWM indices Iu300, Ig500, and Islp

Indices	Iu300	Ig500	Islp	Ieasj
Iu300	1	0.8	0.87	0.5
Ig500		1	0.7	0.6
Islp			1	0.45
Ieasj				1

In the present study, same as many previous work (Zhang et al. 2012; Yao et al. 2019), the thermal condition of SH over the eastern Tibetan Plateau is considered as an external forcing to atmospheric circulations. In fact, the changes in atmospheric circulations may have feedback effect on the thermal conditions over the eastern Tibetan Plateau. Their interaction is an important topic for future research. In addition, the global climate change may also have impact on the decadal variability of SH over CETP and EAWM, which are not dealt with in this study but need further investigation. This analysis has focused on the presence of decadal variability in SH over TP and the atmospheric response, rather than the causing of the variations in wintertime SH. Seasonal snow cover and snow depth during the cold season are affected by the meteorological conditions (Zhang et al. 2016), and play an important role in influencing the ground

thermal regime in cold regions (Zhang 2005). The influence of anomalous snow cover on the plateau's heat flux to the atmosphere shows that the difference of SH between more-snow years (e.g. 1997/98) and less-snow years (e.g. 1996/97) is prominent in spring and is larger than that in winter (Li et al. 2001). However, there is no statistically robust relationship between time series or spatial patterns of the TP winter snow depth and spring SH (Duan et al. 2018). Thus, the relationship between winter SH and snow cover/depth should be carefully considered in future studies.

EAWM is characterized by significant variability at the decadal time scale and although, as discussed in the introduction, several postulated driving mechanisms have been proposed, the research remains inconclusive. Statistical analyses presented herein, to some extent, support the conclusion that the re-amplification of EAWM in recent decades is associated with the strengthening of TP thermal forcing. Further insights into this mechanism could be derived from targeted numerical experiments.

Acknowledgements The authors would like to thank three anomalous reviewers for their constructive comments, which helped greatly in improving this paper. This study was jointly supported by China Postdoctoral Science Foundation (2018M641912), the National Key Research and Development Program (2016YFA0600602), the National Natural Science Foundation of China (41790472), the Special Fund for Tibetan Plateau Research (GYHY201406001) and Fudan University-Tibet University Joint Laboratory For Biodiversity and Global Change. SCP is supported by the US Department of Energy, Office of Science (DE-SC0016438 and DE-SC0016605). The authors wish to acknowledge ECMWF for providing reanalysis products. Output from ERA-Interim is available for download from http://apps.ecmwf.int/datasets/. The authors also acknowledge the provision of high-quality, near-surface data from the China Meteorological Administration (CMA). These near-surface observations are available from http://www.ncc-cma.net/cn/.

References

Bretherton CS, Smith C, Wallace JM (1992) An intercomparison of methods for finding coupled patterns in climate data. J Clim 6:541–560. https://doi.org/10.1175/1520-0442(1998)011<0383:LCTOTO>2.0.CO;2

Chen LX, Reiter ER, Feng ZQ (1985) The atmospheric heat source over the Tibetan Plateau: May-August 1979. Mon Weather Rev 113:1771–1790. https://doi.org/10.1175/1520-0493(1985)113<1771:TAHSOT>2.0.CO;2

Chen W, Hans FG, Huang R (2000) The interannual variability of East Asian Winter Monsoon and its relation to the summer monsoon. Adv Atmos Sci 17(1):48–60

Chen L, Pryor SC, Wang H, Zhang R (2019) Distribution and variation of the surface sensible heat flux over the central and eastern Tibetan Plateau: comparison of station observations and multireanalysis products. J Geophys Res Atmos 124:6191–6206. https://doi.org/10.1029/2018JD030069

Cheung HN, Zhou W, Mok HY, Wu MC (2012) Relationship between Ural–Siberian blocking and the East Asian winter monsoon in relation to the Arctic Oscillation and the El Niño–Southern Oscillation. J Clim 25(12):4242–4257

Cui XP, Sun ZB (1999) East Asian winter monsoon index and its variation analysis. J Nanjing Inst Meteorol 22(3):321–325 (**in Chinese**)

Dee DP, Uppala SM, Simmons AJ, Co-authors (2011) The ERA-Interim reanalysis: configuration and performance of the data assimilation system. Q J R Meteor Soc 137(656):553–597. https://doi.org/10.1002/qj.828

Ding Y (1994) Monsoons over China. Kluwer Academic Publisher, Dordrecht

Ding Y, Krishnamurti TN (1987) Heat budget of the Siberian high and the winter monsoon. Mon Weather Rev 115:2428–2449

Ding Y, Liu Y, Liang S, Ma X, Zhang Y, Si D, Liang P, Song Y, Zhang J (2014) Interdecadal variability of the East Asian winter monsoon and its possible links to global climate change. J Meteorol Res 28(5):693–713

Duan A, Wu G (2008) Weakening trend in the atmospheric heat source over the Tibetan Plateau during recent decades. Part I: Observations. J Clim 21(13):3149–3164. https://doi.org/10.1175/2009JCLI2699.1

Duan A, Li F, Wang M, Wu G (2011) Persistent weakening trend in the spring sensible heat source over the Tibetan Plateau and its impact on the Asian summer monsoon. J Clim 24(21):5671–5682. https://doi.org/10.1175/JCLI-D-11-00052.1

Duan A, Wang M, Lei Y, Cui Y (2013) Trends in summer rainfall over china associated with the Tibetan Plateau sensible heat source during 1980–2008. J Clim 26(1):261–275. https://doi.org/10.1175/JCLI-D-11-00669.1

Duan A, Xiao Z, Wang Z (2018) Impacts of the Tibetan Plateau winter/spring snow depth and surface heat source on Asian summer monsoon: a review. Chin J Atmos Sci 42(4):755–766. https://doi.org/10.3878/j.issn.1006-9895.1801.17247 (**in Chinese**)

Fallah B, Cubasch U, Prömmel K, Sodoudi S (2016) A numerical model study on the behaviour of Asian summer monsoon and AMOC due to orographic forcing of Tibetan Plateau. Clim Dyn 47(5–6):1485–1495. https://doi.org/10.1007/s00382-015-2914-5

Gao R, Zhang R, Wen M, Li T (2019) Interdecadal changes in the asymmetric impacts of ENSO on wintertime rainfall over China and atmospheric circulations over western North Pacific. Clim Dyn 52:7525–7536. https://doi.org/10.1007/s00382-018-4282-4

Ha K-J, Heo K-Y, Lee S-S, Yun K-S, Jhun J-G (2012) Variability in the East Asian monsoon: a review. Meteorol Appl 19:200–215. https://doi.org/10.1002/met.1320

He S, Gao Y, Li F, Wang H, He Y (2017) Impact of Arctic Oscillation on the East Asian climate: A review. Earth-Sci Rev 164:48–62. https://doi.org/10.1016/j.earscirev.2016.10.014

Hu C, Yang S, Wu Q (2015) An optimal index for measuring the effect of East Asian winter monsoon on China winter temperature. Clim Dyn 45:2571–2589. https://doi.org/10.1007/s00382-015-2493-5

Huang R, Chen J, Huang G (2007) Characteristics and variations of the East Asian monsoon system and its impacts on climate disasters in China. Adv Atmos Sci 24(6):993–1023

Huang R, Chen J, Wang L, Lin Z (2012) Characteristics, processes, and causes of the spatio-temporal variabilities of the East Asian monsoon system. Adv Atmos Sci 29(5):910–942. https://doi.org/10.1007/s00376-012-2015-x

Huang R, Liu Y, Feng T (2013) Interdecadal change of summer precipitation over Eastern China around the late-1990s and associated circulation anomalies, internal dynamical causes. Chin Sci Bull 58(12):1339–1349. https://doi.org/10.1007/s11434-012-5545-9

Jhun JG, Lee EJ (2004) A new East Asian winter monsoon index and associated characteristics of the winter monsoon. J Clim 17(4):711–726

Jones PD, Hulme M (1996) Calculating regional climatic time series for temperature and precipitation methods and illustrations. Int J Climatol 16:361–377

Kaiser HF (1958) The varimax criterion for analytic rotation in factor analysis. Psychometrika 23(3):187–200

Kang L, Chen W, Wei K (2006) The interdecadal variation of winter temperature in China and its relation to the anomalies in atmospheric general circulation. Clim Environ Res 11(3):330–339. (**in Chinese**)

Kim JW, An SI, Jun SY, Park HJ, Yeh SW (2017) ENSO and East Asian winter monsoon relationship modulation associated with the anomalous northwest Pacific anticyclone. Clim Dyn 49(4):1157–1179. https://doi.org/10.1007/s00382-016-3371-5

Lau K-M, Li M-T (1984) The monsoon of East Asia and its global associations-a survey. Bull Am Meteorol Soc 65(2):114–125

Lee S, Kim S, Jhun J, Ha K (2013) Robust warming over East Asia during the boreal winter monsoon and its possible causes. Environ Res Lett 8(3):034001. https://doi.org/10.1088/1748-9326/8/3/034001

Li G, Lu J, Jin B, Bu N (2001) The effects of anomalous snow cover of the Tibetan Plateau on the surface heating. Adv Atmos Sci 18(6):1207–1214

Li G, Zhao BJ, Lu JH (2002) Characteristics of bulk transfer coffeicients over the Tibetan Plateau. Acta Meteor Sin 60(1):60–67. (**in Chinese**)

Li D, Wei L, Li W, Lv L, Zhong H, Ji G (2003) The effect of surface sensible heat flux of the Qinghai-Xizang Plateau on general circulation over the Northern Hemisphere and climatic anomaly of China. Clim Environ Res 8(1):60–70 (**in Chinese**)

Luo X, Zhang Y (2015) The linkage between upper-level jet streams over East Asia and East Asian winter monsoon variability. J Clim 28(22):9013–9028. https://doi.org/10.1175/JCLI-D-15-0160.1

Naoto I, Wallace J (1995) Large scale air sea interaction in the Northern Hemisphere from a view point of variations of surface heat flux by SVD analysis.pdf. J Meteorol Soc Japan 73(4):781–794

North GR, Bell TL, Cahalan RF (1982) Sampling errors in the estimation of empirical orthogonal functions. Mon Weather Rev 110(7):699–706. https://doi.org/10.1175/1520-0493(1982)110<0699:SEITEO>2.0.CO;2

Ren X, Yang X, Chu C (2010) Seasonal variations of the synoptic-scale transient eddy activity and Polar Front Jet over East Asia. J Clim 23(12):3222–3233. https://doi.org/10.1175/2009JCLI3225.1

Richman MB (1986) Rotation of principal components. J Climatol 6:293–335

Shi Q, Liang S (2014) Surface-sensible and latent heat fluxes over the Tibetan Plateau from ground measurements, reanalysis, and satellite data. Atmos Chem Phys 14(11):5659–5677. https://doi.org/10.5194/acp-14-5659-2014

Wallace JM, Hobbs PV (2006) Atmospheric science: an introductory survey, 2nd edn. Academic Press, London

Wallace JM, Smith C, Bretherton CS (1992) Singular value decomposition of wintertime sea surface temperature and 500-mb height anomalies. J Clim 5(6):561–576

Wang L, Chen W (2009) Interannual variations of East Asian trough axis at 500 hPa and its association with the East Asian winter monsoon pathway. J Clim 22(3):600–614. https://doi.org/10.1175/2008JCLI2295.1

Wang L, Chen W (2014a) The East Asian winter monsoon: re-amplification in the mid-2000s. Chin Sci Bull 59(4):430–436. https://doi.org/10.1007/s11434-013-0029-0

Wang L, Chen W (2014b) An intensity index for the East Asian winter monsoon. J Clim 27(6):2361–2374. https://doi.org/10.1175/JCLI-D-13-00086.1

Wang H, Li D (2019) Decadal variability in summer precipitation over eastern China and its response to sensible heat over the Tibetan Plateau since the early 2000s. Int J Climatol 39:1604–1617. https://doi.org/10.1002/joc.5903

Wang L, Lu M (2017) The East Asian winter monsoon. In: C-P C, H-C K, N-C L, R H J, B W and M W (eds) The global monsoon system: research and forecast (3rd Edition). World Scientific Publishing Co., Pte. Ltd., 51–61. https://doi.org/10.1142/9789813200913

Wang A, Wang Q (1985) The effects of the Qinghai-Xizang Plateau on the mean general circulation in East Asia in winter. Plateau Meteorol 4(2):109–120 (**in Chinese**)

Wang L, Huang R, Gu L, Chen W, Kang L (2009) Interdecadal variations of the East Asian winter monsoon and their association with quasi-ttationary planetary wave activity. J Clim 22(18):4860–4872. https://doi.org/10.1175/2009JCLI2973.1

Wang B, Wu Z, Chang CP, Liu J, Li J, Zhou L (2010) Another look at interannual-to-interdecadal variations of the East Asian winter monsoon: the northern and southern temperature modes. J Clim 23(6):1495–1512. https://doi.org/10.1175/2009JCLI3243.1

Wilks DS (2011) Statistical methods in the atmospheric sciences, 3rd edn. Oxford, Academic Press

Wu G, Liu Y, Wang T, Wan R, Liu X, Li W, Wang Z, Zhang Q, Duan A, Liang X (2007) The influence of mechanical and thermal forcing by the Tibetan Plateau on Asian climate. J Hydrometeorol 8(4):770–789. https://doi.org/10.1175/JHM609.1

Xie J, Yu Y, Li JL, Ge J, Liu C (2018) Comparison of surface sensible and latent heat fluxes over the Tibetan Plateau from reanalysis and observations. Meteor Atmo Phys. https://doi.org/10.1007/s00703-018-0595-4

Xu L, Gao H, Li YQ (2009) Sensible heating over the Tibetan Plateau linked to the onset of Asian monsoon. Atmos Oceanic Sci Lett 2(6):350–356. https://doi.org/10.1080/16742834.2009.11446833

Yanai M, Li CF, Song ZS (1992) Seasonal heating of the Tibetan Plateau and its effects on the evolution of the Asian summer monsoon. J Meteorol Soc Jpn 70(1):189–221. https://doi.org/10.2151/jmsj1965.70.1B_319

Yang X, Li D (2009) Variation of winter temperature in China and its responding to the anomalies in East Asian winter monsoon and surface heating field over Qinghai-Xizang Plateau. Plateau Meteor 28(4):731–737. (**in Chinese**)

Yang K, Guo X, Wu B (2011) Recent trends in surface sensible heat flux on the Tibetan Plateau. Sci China Earth Sci 54(1):19–28. https://doi.org/10.1007/s11430-010-4036-6

Yao T, Xue Y, Chen D, Coauthors (2019) Recent Third Pole's rapid warming accompanies cryospheric melt and water cycle intensification and interactions between monsoon and environment: multi-disciplinary approach with observation, modeling and analysis. Bull Am Meterol Soc 100:423–444. https://doi.org/10.1175/BAMS-D-17-0057.1

Ye D, Gao Y (1979) Meteorology of the Qinghai-Xizang (Tibet) Plateau. Science Press, Beijing (**in Chinese**)

Ye D, Wu G (1998) The role of the heat source of the Tibetan Plateau in the general circulation. Meteorol Atmos Phys 67(1–4):181–198. https://doi.org/10.1007/BF01277509

Yeh TC (1950) The circulation of the high troposphere over China in the winter of 1945–46. Tellus 2(3):173–183. DOI:https://doi.org/10.3402/tellusa.v2i3.8548

Zhang T (2005) Influence of the seasonal snow cover on the ground thermal regime: an overview. Rev Geophys. https://doi.org/10.1029/2004RG000157

Zhang Y, Sperber KR, Boyle JS (1997) Climatology and interannual variation of the East Asian winter monsoon: Results from the 1979-95 NCEP/NCAR reanalysis. Mon Wea Rev 125:2605–2619

Zhang Y, Xiao C (2013) Variability modes of the winter upper-level wind field over Asian mid- high latitude region. Atmos Oceanic Sci Lett 6(5):295–299. https://doi.org/10.3878/j.issn.1674-2834.12.0104

Zhang J, Zhu B, Zhu F, Weng D, Sun G, Lv J, Peng Y, Wang Y (1988) Advances in the Qinghai-Xizang Plateau meteorolory—the Qinghai-Xizang Plateau meteorological experiment (1979) and research. Science Press, Beijing (**in Chinese**)

Zhang R, Koike T, Xu X, Ma Y, Yang K (2012) A China-Japan cooperative JICA atmospheric observing network over the Tibetan

Plateau (JICA/Tibet Project): an overview. J Meteor Soc Jpn 90C:1–16. https://doi.org/10.2151/jmsj.2012-C01

Zhang R, Zhang R, Zuo Z, Li W (2016) Temporal and spatial features and inter-annual variability of wintertime snow mass balance over China. Int J Climatol 36:3897–3390. https://doi.org/10.1002/joc.4599

Zhou X, Zhao P, Chen J, Chen L, Li W (2009) Impacts of thermodynamic processes over the Tibetan Plateau on the Northern Hemispheric climate. Sci China Ser D-Earth Sci 39(11):1473–1486. https://doi.org/10.1007/s11430-009-0194-9

Zhu X, Liu Y, Wu G (2012) An assessment of summer sensible heat flux on the Tibetan Plateau from eight data sets. Sci China Earth Sci 55(5):779–786. https://doi.org/10.1007/s11430-012-4379-2

Zhu L, Huang G, Fan G, Qu X, Zhao G, Hua W (2017) Evolution of surface sensible heat over the Tibetan Plateau under the recent global warming hiatus. Adv Atmos Sci 34(10):1249–1262. https://doi.org/10.1007/s00376-017-6298-9